

Nonlocal, Flat-Band Meta-Optics for Monolithic, High-Efficiency, Compact Photodetectors

Minho Choi, Christopher Munley, Johannes E. Fröch, Rui Chen, and Arka Majumdar*



Cite This: <https://doi.org/10.1021/acs.nanolett.3c05139>



Read Online

ACCESS |



Metrics & More



Article Recommendations

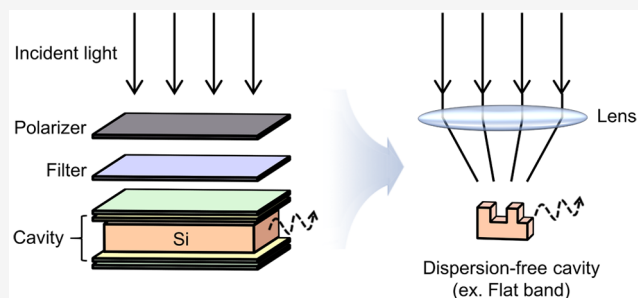


Supporting Information

ABSTRACT: Miniaturized photodetectors are becoming increasingly sought-after components for next-generation technologies, such as autonomous vehicles, integrated wearable devices, or gadgets embedded on the Internet of Things. A major challenge, however, lies in shrinking the device footprint while maintaining high efficiency. This conundrum can be solved by realizing a nontrivial relation between the energy and momentum of photons, such as dispersion-free devices, known as flat bands. Here, we leverage flat-band meta-optics to simultaneously achieve critical absorption over a wide range of incidence angles. For a monolithic silicon meta-optical photodiode, we achieved an ~ 10 -fold enhancement in the photon-to-electron conversion efficiency. Such enhancement over a large angular range of $\sim 36^\circ$ allows incoming light to be collected via a large-aperture lens and focused on a compact photodiode, potentially enabling high-speed and low-light operation. Our research unveils new possibilities for creating compact and efficient optoelectronic devices with far-reaching impact on various applications, including augmented reality and light detection and ranging.

KEYWORDS: meta-optics, photodetector, flat band, nonlocal, guided mode resonance

Absorption of light and the conversion of photons into other forms of energy, such as excitons and phonons, have been widely utilized for optical sensing,^{1,2} imaging,³ and energy harvesting.⁴ Recently, rapid developments in wearable devices and emergence of the Internet of Things have further increased the demand for smaller photodetectors (PDs) with high absorption efficiency.^{5,6} Compact integrated PDs could potentially provide several advantages for these applications, including high-resolution imaging thanks to the large pixel count,^{7,8} reduced energy consumption,⁹ and high-speed operation.¹⁰ However, two major limitations impede their functionalities: a small device footprint limits the total light collection, and a small device thickness limits the total amount of absorbed light (Figure 1a). The first issue can be alleviated using a lens with large aperture to collect light from a wider area,¹¹ while an optical cavity can circumvent the latter problem.¹² Resonant cavity-enhanced absorption occurs as the optical cavity traps light for a longer time period, which increases the absorption efficiency. Various dielectric and plasmonic resonators have been used to enhance the photon-to-electron conversion efficiency of PDs in silicon^{9,13,14} and other materials.^{15–18} However, these results all focus on normal incident light and thus are incompatible with lens-based concentrators (Figure 1b), as focused light contains a wide range of incidence angles. Therefore, an angle-independent resonant cavity can both enhance the light absorption and be compatible with a light concentrator to enhance the photoresponsivity (Figure 1c).



Such enhancement over a large angular range of $\sim 36^\circ$ allows incoming light to be collected via a large-aperture lens and focused on a compact photodiode, potentially enabling high-speed and low-light operation. Our research unveils new possibilities for creating compact and efficient optoelectronic devices with far-reaching impact on various applications, including augmented reality and light detection and ranging.

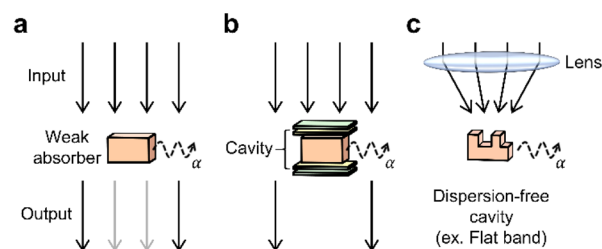


Figure 1. Schematics of light absorption in a weak absorber. (a) Absorption from a weak absorber itself. (b) Conventional cavity-enhanced absorption matching with a certain angle of incoming light. (c) Flat-band-enhanced absorption matching with a wide range of incident angle of incoming light, making it possible to use a concentrator to capture a large amount of light.

The flat-band concept was first conceived in condensed matter physics^{19–21} and has only recently been applied to photonics in various forms.^{22–27} However, to this point, photonic flat bands have remained merely an interesting

Received: December 29, 2023

Revised: February 27, 2024

Accepted: February 28, 2024

physical phenomenon without clear applications. Their unique property, an angle-independent resonance frequency, allows cavity-enhanced absorption of light consisting of many incident angles. We adapt a guided-mode resonance design in a silicon meta-optic and, by fine-tuning the geometrical parameter, implement a photonic flat band.^{28–31} By exploiting the inherent absorption of silicon in the near-infrared, we reach critically coupled absorption with an absorption ratio (α) of about 70% by adjusting the quality (Q) factor while maintaining the flat band. This ensures that light over a wide angular range ($\pm 18^\circ$) undergoes cavity-enhanced absorption.

To harness the advantage of the enhanced absorption, we designed and fabricated a monolithic lateral p-i-n PD within flat-band meta-optics. This enables the collection of a large amount of light by using a lens while keeping the active volume small. Thus, we achieved both a light concentration using a larger aperture and cavity enhancement over a large angular range. For incident light focused with a numerical aperture (NA) of 0.13, the flat-band-based PD shows a 10.3-fold enhanced responsivity compared to the unpatterned Si-PD at the resonance wavelength of ~ 785 nm. In addition, the responsivity of this single-junction meta-optical PD depends on the wavelength and polarization of light, which can be further exploited to create a spectrally selective and polarization-sensitive miniaturized PD. Such multifunctionality can reduce the fabrication costs and optical crosstalk between pixels⁹ and have far-reaching impact on wearable sensors, including miniature spectrometers and Li-Fi transducers.^{32–35}

Cavity-enhanced absorption in conventional resonators retains a strong chromatic dependence due to the optical path length dependence on the incidence angle. Specifically, the resonance conditions arise from constructive/destructive interference, and thus a variation in the effective optical path length drastically alters it. On the contrary, photonic flat bands have no such chromatic dispersion over a certain angular range. By fine-tuning the coupling between different modes, various photonic bands including flat-band, Dirac-cone, and multivalley structures have been realized in nonlocal meta-optics.²⁸ By breaking the vertical symmetry through sub-wavelength patterning, such a meta-optic can also couple efficiently to the free space.^{28–31} Guided by these design insights, we created a flat-band one-dimensional (1D) meta-optic in a partially etched silicon slab on sapphire (Figure 2a). The unit cell is composed of two symmetry broken meta-atoms. While the thickness of the silicon film is fixed at 230 nm, other parameters, including the fill factor, partial etch ratio, asymmetry (Δ) between the adjacent meta-atoms, and period, constitute the design space (Figure 2b). Both the fill factor and partial etching ratio introduce a vertical symmetry breaking, while Δ and period control the Q factor and the resonance frequency, respectively. We designed the flat-band meta-optics using rigorous coupled-wave analysis (RCWA) and fabricated the structure via single-step electron beam lithography, followed by reactive ion etching (Figure S1 in the Supporting Information). Scanning electron microscopy images of the fabricated structure are shown in Figure 2c. Using a high-NA objective lens and high-resolution spectrometer, we set up energy-momentum spectroscopy and measured the photonic band structures (Figure S3 in the Supporting Information). By adjusting the fill factor of the structure, we realized various photonic band structures including a dispersive band and a dispersion-free photonic flat band near the gamma-point ($k_x = k_y = 0$), as shown in

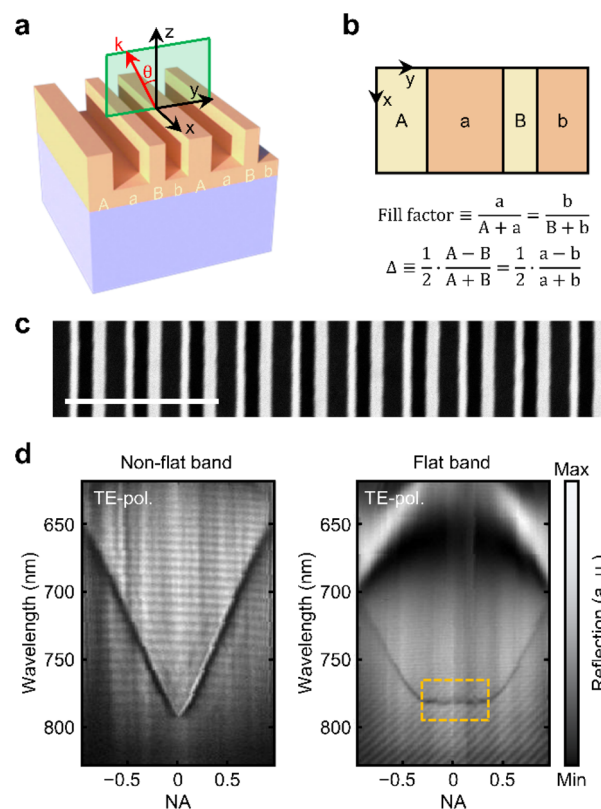


Figure 2. Implementation of photonic flat band as an angle-independent resonator. (a) Schematic of a flat band meta-optic which has a wide range of angle, θ , independent response. (b) Top view of the meta-optics consisting of four different parts due to the partial etching and definitions of fill factor and asymmetry factor, Δ . (c) Scanning electron microscope image of the flat band meta-optic. Scale bar: 1.0 μm . (d) Reflective energy-momentum spectra of the meta-optics: dispersive band and dispersion-free flat band near the gamma-point, respectively. A yellow dashed box indicates the flat band.

Figure 2d and Figure S4 in the Supporting Information. Noticeably, the flat band emerges with an isofrequency resonance in the near-infrared region (~ 780 nm) and is maintained over a wide angular range of $\pm 18^\circ$. In comparison, other resonators show a strong dependence of the resonance frequency on the angle of incidence.

To understand how the photonic flat band can be leveraged to maximize the absorption efficiency, we consider a configuration of two partially reflecting mirrors and a weak thin-film absorber in between (Figure 3a). In this analogy, the flat-band meta-optic is equivalent to a curved cavity, which facilitates cavity-enhanced absorption simultaneously for a wide angular range of incident light (Figure 3b). The boundary conditions, however, to maximize the absorption inside the cavity are not trivial, and simply maximizing the Q factor or increasing the absorption coefficient of the device would not directly maximize the absorption. Therefore, to predict whether the flat-band meta-optic exhibits critically coupled absorption, we modeled the system behavior using the finite-difference time-domain (FDTD) method (see details in the Supporting Information). We studied both the reflective and transmissive response of the meta-optics using a model complex refractive index, $3.7 + i\kappa$, for the crystalline silicon. For a zero-absorption coefficient, i.e., $\kappa = 0$, we clearly observe a Fano-like resonance from both reflection and transmission

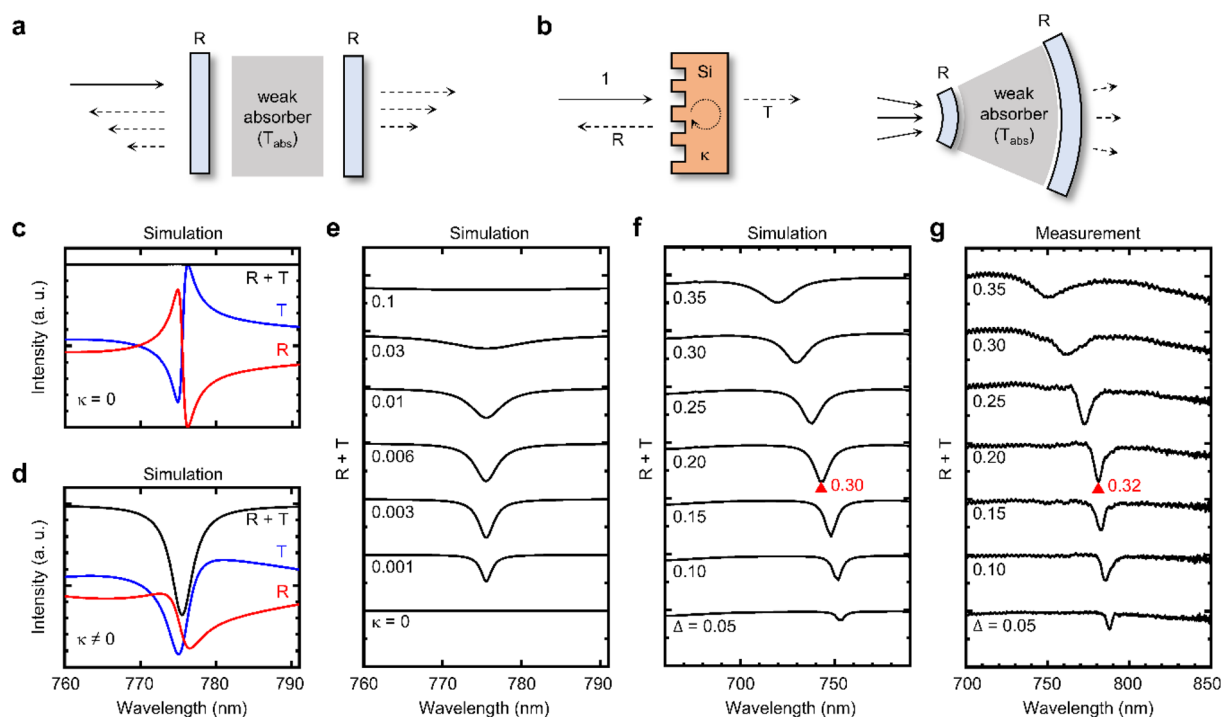


Figure 3. Flat-band meta-optic and critically coupled absorption. (a) Conventional optical resonator with a weak absorber inside. (b) Interpretation of the flat-band meta-optics as a cavity and a weak absorber. (c, d) Simulated reflection, R , and transmission, T , spectra of the flat-band meta-optics without and with absorption, respectively. (e, f) Simulated absorption spectra with respect to κ and Δ , respectively. (g) Experimentally measured absorption spectra with respect to Δ . Here, we used the fill factor, partial etching ratio, and period values of 0.78, 0.84, and 384 nm, respectively, for the meta-optics parameters, while varying the Δ value.

spectra, and no absorption occurs at any wavelength (Figure 3c). On the other hand, if there is a finite value of κ , the Fano-like resonance becomes weaker, and clear cavity-assisted absorption occurs (Figure 3d). As we gradually increase κ , from 0 to 0.1, the meta-optic meets the critically coupled absorption point at $\kappa \approx 0.005$ with an α value of about 70%, which is much higher than that of a GMR structure with a higher κ value of 0.1, where α is about 25% (Figure 3e and Figure S6a in the Supporting Information).

In practice, κ is an intrinsic property and has a fixed value; thus, other factors have to be adjusted to reach the critical absorption condition. Fortunately, we can fine-tune the cavity Q factor by adjusting the asymmetry, Δ , of the structure—as the value of Δ decreases, the resonance becomes narrower, as a bound-state-in-continuum resonance.^{29,30} From FDTD simulations with the measured refractive index, we can obtain a Q factor of about 174 at $\Delta \approx 0$, while the Q factor decreases gradually as Δ increases and reaches ~ 50 for $\Delta = 0.26$ (Figure S6b in the Supporting Information). By gradually changing the Δ value of the structure from 0 to 0.35 in simulation, we can find the critically coupled absorption point near $\Delta = 0.20$, where α is about 70%, consistent with the simulated result of varying κ (Figure 3f). The measured results are consistent with the simulation, as we can see the change in the cavity resonance and line width as Δ increases from 0.05 to 0.20 (Figure S6f in the Supporting Information). We measured both reflection (R) and transmission (T) spectra of the meta-optics with varying Δ , and the sum of normalized reflection and transmission is shown in Figure 3g. We measure $\alpha \approx 68\%$ at the critical coupling condition, which is similar to the simulated value of $\sim 70\%$. Theoretical explanations are shown in Section 3 in the Supporting Information.

We note that $\sim 60 \mu\text{m}$ thick silicon and antireflection coating are needed to achieve 70% absorption without cavity enhancement at $\sim 750 \text{ nm}$ wavelength, where silicon has an absorption coefficient of around 0.014. Such a thick medium hinders fabrication availability and also reduces the operation speed of the device due to the long distance carriers have to travel. But with the cavity enhancement, only a 230 nm thick silicon can achieve the same amount of absorption. On the other hand, we can tune the resonant wavelength of the flat-band meta-optic by adjusting the structural parameters. In detail, silicon generally has a lower absorption coefficient at longer wavelengths; then the Q factor of the structure needs to be enhanced which corresponds to a decrease in Δ (Section 3 in the Supporting Information).

We demonstrate a compact, high-responsivity PD using the optimized silicon flat-band meta-optic, exploiting the critically coupled absorption over a wide angular range of incident light. This enables us to significantly increase the total light collection as compared to other cavity-enhanced PDs.^{9,13–18} As shown in Figure 4a, a lens on top of a compact, single-junction PD can be used to increase the amount of light collected and absorbed into a single PD.

Using an additional lithography step, we selectively doped the silicon meta-optic and created a lateral p-i-n PD with a $10 \mu\text{m}$ wide intrinsic region. Figure 4b shows images of multiple PDs connected to metal pads and wires (Figure S7 in the Supporting Information). To rule out variations and to clarify the effect of flat-band meta-optics compared to others, i.e. unpatterned silicon films and “non-flat-band” meta-optics, we fabricated multiple devices in a row and put a pair of large metal pads to connect the p- and n-doped regions of all devices. In a single chip, 14 devices were connected with large

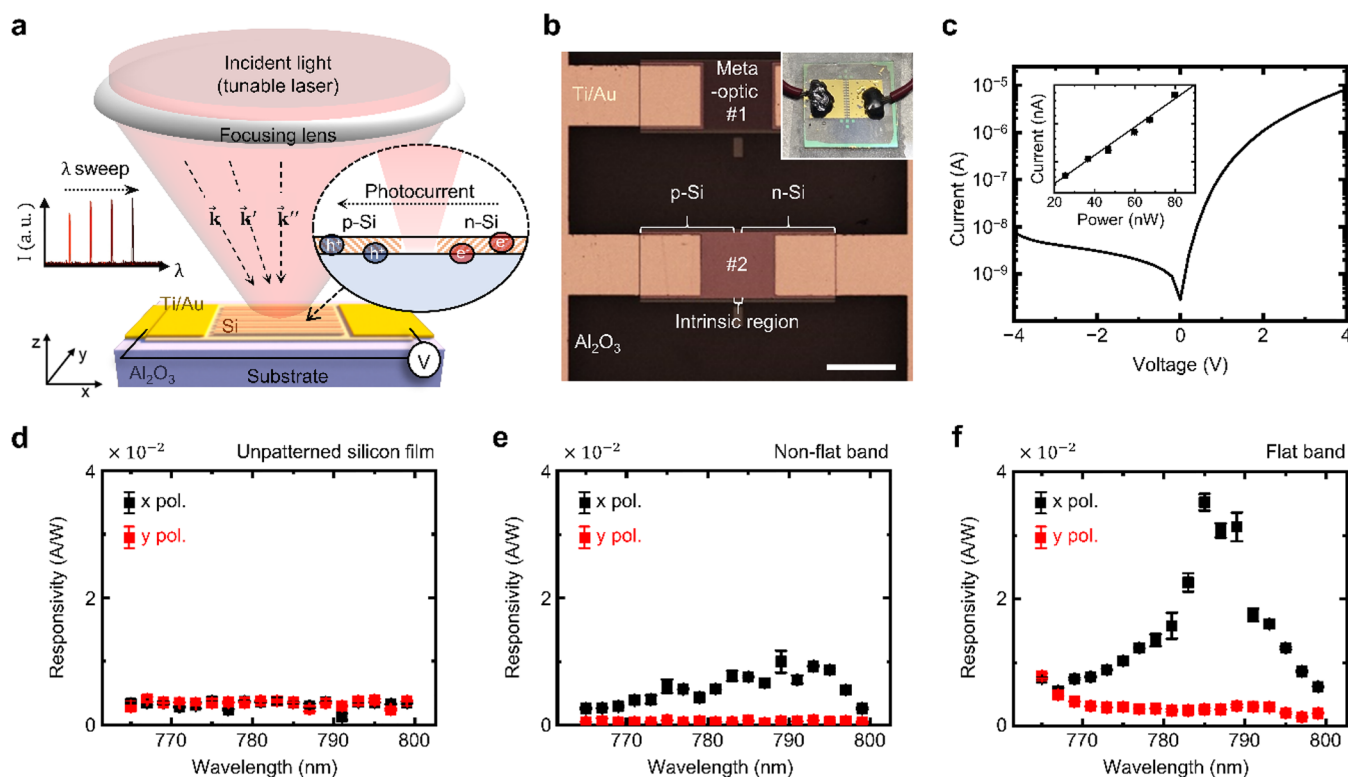


Figure 4. Lateral p-i-n PD with flat-band meta-optics. (a) Schematics of the lateral p-i-n PD using flat-band meta-optics. Large amounts of light are collected and focused onto a compact flat-band-based PD by a lens. A tunable laser allows wavelength-selective response measurement of devices. (b) Optical microscope image of the device. The inset image shows the actual device after the wires are soldered to the metal pads. The length of the scale bar is 200 μm . (c) I - V curve of the PD without incident light. The inset graph shows the current as a function of the incident light power. The slope of the linear fit indicates the responsivity, η , of the device. (d-f) Wavelength- and polarization (pol.)-dependent η values of the PDs made of (d) 230 nm thick unpatterned silicon film, (e) meta-optic with “non-flat-band” photonic structure, and (f) meta-optic with photonic flat-band structure. The photonic band structure of “non-flat-band” is represented in Figure 2d.

metal pads at the same time. Figure 4c shows an I - V characteristic of the entire chip from -4 to 4 V, with less than 10 nA of leakage current at reverse bias voltage and a clear rectification behavior of the diode. Considering the number of devices on the chip, we can estimate that each single device has a leakage current of less than 1 nA at a reverse bias voltage of -4 V or less. We note that the low dark current originated from small photosensitive volume, i.e., $0.2 \times 0.01 \times 0.00023$ mm, based on a thin, lateral p-i-n junction. But even with a small photosensitive volume, we can collect a large amount of light using a concentrator and focus onto the active area. Additionally, we can increase the photosensitive volume if we create a vertical p-i-n junction out of the thin silicon film.

We focused light with an NA of 0.13 to an intrinsic region of the device and measured the photocurrent, which is linearly proportional to the optical power of the incident light, at a reverse bias voltage of -2 V (Figure 4c). Here, the slope of the linearly fitted line gives us the responsivity (η) of the PD, which represents the conversion efficiency from photon energy to electrical current. We note that this monolithic silicon PD could generate photocurrent from a few tens of nanowatt light. An experimental setup for the photocurrent measurement is shown in Figure S8 in the Supporting Information.

We then measured a series of power-dependent photocurrents to extract η while adjusting the polarization and laser wavelength from 765 to 799 nm in 2 nm steps. The photocurrent measurement was repeated five times to obtain an average value. As shown in Figure 4d, the average values of

η for a 230 nm thick unpatterned silicon film are 3.2 ± 0.2 and 3.4 ± 0.1 mA/W for x - and y -polarized light along the wavelength from 765 to 799 nm, respectively. There was no clear trend in the wavelength or polarization direction. On the contrary, we can observe the wavelength and polarization dependence in η for a meta-optic with “non-flat-band” photonic structure (Figure 4e). The average values of η are 5.7 ± 0.4 and 0.5 ± 0.1 mA/W for x - and y -polarized light along the 765 to 799 nm wavelength, respectively. It shows an enhanced η value for x -polarized light at a wide range of wavelengths from 773 to 795 nm and had a maximum value of $\eta = 10 \pm 2$ mA/W at the 789 nm wavelength. However, this enhancement occurred only for x -polarized light, while even a reduction occurred for y -polarized light compared to the unpatterned silicon film because the meta-optic has less absorptive material after the patterned etching.

As shown in Figure 4f, for the flat-band meta-optic, we observed a much stronger and sharper enhancement of η , as the resonance wavelength remains the same over a wide range of incident angles. The average values of η for the HCG structure with a flat band are 15 ± 0.7 and 3.1 ± 0.1 mA/W for x - and y -polarized light along the 765 to 799 nm wavelength, respectively. It shows a strongly enhanced η for x -polarized light at wavelengths near 785 nm, with a maximum value of $\eta = 35 \pm 1$ mA/W at 785 nm wavelength. All the measured data for flat-band-based PD are shown in Figure S9 in the Supporting Information. The resonance wavelength of ~ 785 nm is well-matched with the measured photonic band structure

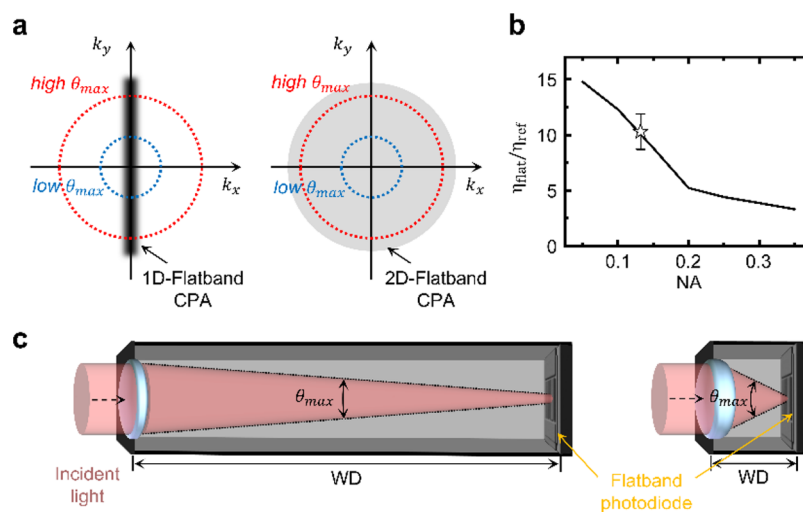


Figure 5. NA-dependent absorption in the 1D flat band. (a) Regions of incident light with high (red)- and low-NA (blue) focusing lens and areas of 1D and 2D flat band in lateral k -space. (b) Simulated absorption power enhancement of 1D flat band compared to the 230 nm thick silicon film depends on NA of the focused input light. A star symbol indicates the measured value at NA - 0.13. (c) Schematics of the flat-band-based PD with different NA of the concentrators and fixed aperture size.

of the flat band (Figure S10 in the Supporting Information). We note that the higher η values compared to the non-flat-band meta-optic occur due to the lower fill factor of the flat-band structure and therefore more absorptive material.

Overall, we achieve an enhancement in η for the flat-band-based PD, given as $\eta_{flat}/\eta_{film} = 10.3 \pm 1.6$ and $\eta_{flat}/\eta_{nonflat} = 3.5 \pm 0.7$ in comparison to the unpatterned silicon film and the non-flat-band meta-optic, respectively. The flat-band-based PD has a highly dependent η with respect to both wavelength and polarization, where the full-width half-maximum of the wavelength-enhancement region is ~ 10 nm and the extinction ratio of orthogonal, linear polarization is 0.86 ± 0.09 . From FDTD simulations, the Q factor of the meta-optic is around 76 at $\Delta = 0.20$ (Figure S6b in the Supporting Information), which matches well with the enhanced response bandwidth of the PD. In this regards, the flat-band-based PD can be considered an integrated PD with a wavelength-selective filter and linear polarization sensitivity, essentially combining three functionalities into a single meta-optic, free of complex fabrication and optical crosstalk between optics.⁹

Moreover, we simulated the NA-dependent absorption from the 230 nm thick unpatterned silicon film as a reference to extract the absorption enhancement factor (Z) of the flat-band meta-optic. In general, we can achieve higher Z for lower NA of the focused light because our 1D flat band only covers 1D k -vectors, while the focused light has two-dimensional (2D) k -vectors (Figure 5a). In section 4 in the Supporting Information, we discuss creating a rotationally symmetric meta-optics to extend the flat band from 1D to 2D. However, there are a few drawbacks for the 2D flat band. First, a precise alignment becomes necessary unlike the case for the 1D flat band, because the light needs to be focused exactly on the rotational center. Second, only 50% of the incoming light can match with the flat-band resonance due to the polarization selection (details in Section 5 in the Supporting Information). Our 1D flat band has strong linear polarization selectivity and wavelength sensitivity at the same time, which a 2D flat band cannot have.

Then, we compared the simulated enhancement factor, Z , and measured enhancement factor, η_{flat}/η_{film} , at the resonance

wavelength of the 1D flat band. Here, Z is a term that describes only the light absorption but can be compared to the PD efficiency enhancement factor, η_{flat}/η_{film} . This is because the amount of light absorption is proportional to the generated free carrier density which corresponds to the photocurrent amplitude under a reverse bias voltage. Since all the PDs, including the unpatterned silicon film, non-flat-band meta-optic, and flat-band meta-optic, share the same electrical components (i.e., contact pads and voltage source), we can assume that the conversion efficiency from free carriers to photocurrents is the same for all PDs. At an NA of 0.13, the simulated Z and experimentally measured η_{flat}/η_{film} are in good agreement, $Z = 10.4$ and $\eta_{flat}/\eta_{film} = 10.3 \pm 1.6$ (Figure 5b). For an NA value lower than 0.13, we can achieve even higher enhancement, but the volume of the total system will be larger when the aperture size, which corresponds to the light concentration amount, remains the same (Figure 5c).

The measured responsivity, η , of the flat-band meta-optical PD is about 0.04 A/W at its resonance wavelength of 785 nm, corresponding to a quantum efficiency (QE) of about 6%. Although this value is smaller than those of current state-of-the-art commercial silicon PDs,³⁶ which have QE values of $\sim 95\%$, and a widely used commercial CMOS camera, i.e. Thorlabs CS165MU, which has a QE of $\sim 35\%$ in the near-infrared region, our flat-band-based PD has an order of magnitude smaller thickness. This could potentially provide advantages in terms of supply voltage (< 2 V), dark current (< 1 nA), and response speed (< 100 ps) with a small active area. We envision that this value could be further boosted by further optimization of the p-i-n junction parameters (e.g., active layer width, doping concentration, and annealing temperature)^{37,38} or by adding a photoconductive gain with a CMOS-compatible process.³⁹ Nevertheless, our approach demonstrates how a photonic flat band can be exploited to enhance the light absorption for focused, incident light, as we achieve a 10.3-fold enhancement from the flat-band-based PD for focused light of NA 0.13 compared to an unpatterned silicon-film-based PD.

In addition, our flat-band meta-optical PD provides wavelength-selective and polarization-selective responses, both of which are adjustable through the specific design

parameters. The linear polarization selectivity of the device can be modulated by the device orientation, and the wavelength selectivity can be adjusted by the period of the structure or changing the effective refractive index of the structure (e.g., by integrating phase-change materials with the meta-optics).^{40,41} By tuning the resonance frequency of the flat band, meta-optic spectral information on the incident light can be collected by a single PD, which is equivalent to a compact spectrometer. In the case of conventional photonic band structures rather than a photonic flat band, the resonance frequency varies greatly depending on the incident angle of light; therefore, it is difficult to confirm the wavelength of measured light unless the incoming light has a certain incident angle, e.g., normal incidence. In comparison, the photonic flat band maintains its resonance frequency, irrespective of the incident angle.

We realized cavity-enhanced absorption using a single flat-band meta-optic with absorption power of 68% for a wide angular range of NA 0.35, which is about 25 times more than the previous angular resolution of angle-independent cavities using bulk optics.⁴² We utilized this silicon flat-band meta-optic as an efficient and compact PD. This flat-band-based PD can provide improved absorption over a wide range of angles of incidence, allowing light collection with a large aperture in small footprint PD. Due to the 1D characteristics of the flat band, it has a particular k -vector and linear polarization dependence, which results in NA-dependent absorption enhancement. Hence, we can consider this flat-band-based PD as a miniaturized PD which has wavelength and polarization filter insertions. This work, which is not limited to silicon materials, showcases the first practical application of the photonic flat band as a degenerate resonant cavity-enhanced absorber, with potential impacts in fields requiring wavelength-selective compact detectors or angle-insensitive detectors.

■ ASSOCIATED CONTENT

Data Availability Statement

All data needed to evaluate the conclusions in the paper are present in the paper and/or the [Supporting Information](#). The data that support other findings of this study are available from the corresponding author on request.

SI Supporting Information

The Supporting Information is available free of charge at <https://pubs.acs.org/doi/10.1021/acs.nanolett.3c05139>.

Experimental details, RCWA simulation of angle-dependent transmission spectra in meta-optics, electric-field profile of the guided-mode resonators, schematic of the experimental setup for the energy-momentum spectrum measurement, energy-momentum spectra of the meta-optic, critically coupled absorption from a weak absorber and an optical resonator, critically coupled absorption of the flat-band meta-optics, schematic procedure for creating a lateral p-i-n photodiode from the silicon, flat-band meta-optics, schematic of the experimental setup for meta-optics photodiode characterization, wavelength-dependent responsivity of the flat-band photodiode for focused light with NA 0.13, energy-momentum spectrum of the flat-band photodiode in reflection configuration, NA-dependent absorption in 2D bullseye structure compared to 1D flat band, energy-momentum spectra of the 2D bullseye structure, and

parameters to convert 1D flat band to 2D bullseye structure ([PDF](#))

■ AUTHOR INFORMATION

Corresponding Author

Arka Majumdar – Department of Electrical and Computer Engineering, University of Washington, Seattle, Washington 98195, United States; Department of Physics, University of Washington, Seattle, Washington 98195, United States; orcid.org/0000-0003-0917-590X; Email: arka@uw.edu

Authors

Minho Choi – Department of Electrical and Computer Engineering, University of Washington, Seattle, Washington 98195, United States; orcid.org/0000-0002-4497-2763

Christopher Munley – Department of Physics, University of Washington, Seattle, Washington 98195, United States; orcid.org/0000-0001-5684-3144

Johannes E. Fröch – Department of Electrical and Computer Engineering, University of Washington, Seattle, Washington 98195, United States; Department of Physics, University of Washington, Seattle, Washington 98195, United States

Rui Chen – Department of Electrical and Computer Engineering, University of Washington, Seattle, Washington 98195, United States; orcid.org/0000-0001-8492-729X

Complete contact information is available at:

<https://pubs.acs.org/10.1021/acs.nanolett.3c05139>

Author Contributions

M.C. and A.M. conceptualized the project. M.C. and C.M. designed, M.C., J.E.F., and R.C. fabricated, and M.C. measured the devices. M.C. and C.M. analyzed the data. M.C. visualized the data. A.M. supervised the project. M.C. wrote the original draft of the manuscript, and all the authors worked on review and editing.

Notes

The authors declare no competing financial interest.

■ ACKNOWLEDGMENTS

This material is based upon work supported by the National Science Foundation Grant No. DMR-2019444. Part of this work was conducted at the Washington Nanofabrication Facility/Molecular Analysis Facility, a National Nanotechnology Coordinated Infrastructure (NNCI) site at the University of Washington with partial support from the National Science Foundation via awards NNCI-1542101 and NNCI-2025489.

■ REFERENCES

- (1) Kim, I.; Kim, W.-S.; Kim, K.; Ansari, M. A.; Mehmood, M. Q.; Badloe, T.; Kim, Y.; Gwak, J.; Lee, H.; Kim, Y.-K.; Rho, J. Holographic metasurface gas sensors for instantaneous visual alarms. *Sci. Adv.* **2021**, *7*, No. eabe9943.
- (2) Ma, C.; Yuan, S.; Cheung, P.; Watanabe, K.; Taniguchi, T.; Zhang, F.; Xia, F. Intelligent infrared sensing enabled by tunable moiré quantum geometry. *Nature* **2022**, *604*, 266–272.
- (3) Wang, H.; Lee, D.; Cao, Y.; Bi, X.; Du, J.; Miao, K.; Wei, L. Bond-selective fluorescence imaging with single-molecule sensitivity. *Nat. Photonics* **2023**, *17*, 846–855.
- (4) Chen, J.; Yang, Y.; Dong, H.; Li, J.; Zhu, X.; Xu, J.; Pan, F.; Yuan, F.; Dai, J.; Jiao, B.; Hou, X.; Jen, A. K.-Y.; Wu, Z. Highly efficient and stable perovskite solar cells enabled by low-dimensional perovskitoids. *Sci. Adv.* **2022**, *8*, No. eabk2722.

- (5) Wu, J.; Guo, Y.; Deng, C.; Zhang, A.; Qiao, H.; Lu, Z.; Xie, J.; Fang, L.; Dai, Q. An integrated imaging sensor for aberration-corrected 3D photography. *Nature* **2022**, *612*, 62–71.
- (6) Jang, H.; Hinton, H.; Jung, W.-B.; Lee, M.-H.; Kim, C.; Park, M.; Lee, S.-K.; Park, S.; Ham, D. In-sensor optoelectronic computing using electrostatically doped silicon. *Nat. Electron.* **2022**, *5*, 519–525.
- (7) Fu, P.; Cao, W.; Chen, T.; Huang, X.; Le, T.; Zhu, S.; Wang, D.-W.; Lee, H. J.; Zhang, D. Super-resolution imaging of non-fluorescent molecules by photothermal relaxation localization microscopy. *Nat. Photonics* **2023**, *17*, 330–337.
- (8) Cai, G.; Li, Y.; Zhang, Y.; Jiang, X.; Chen, Y.; Qu, G.; Zhang, X.; Xiao, S.; Han, J.; Yu, S.; Kivshar, Y.; Song, Q. Compact angle-resolved metasurface spectrometer. *Nat. Mater.* **2024**, *23*, No. 71.
- (9) Ho, J.; Dong, Z.; Leong, H. S.; Zhang, J.; Tjiotharsono, F.; Daqiqeh Rezaei, S.; Goh, K. C. H.; Wu, M.; Li, S.; Chee, J.; Wong, C. P. Y.; Kuznetsov, A. I.; Yang, J. K. W. Miniaturizing color-sensitive photodetectors via hybrid nanoantennas toward submicrometer dimensions. *Sci. Adv.* **2022**, *8*, No. eadd3868.
- (10) Gao, Y.; Cansizoglu, H.; Polat, K. G.; Chandiparsi, S.; Kaya, A.; Mamtaz, H. H.; Mayet, A. S.; Wang, Y.; Zhang, X.; Yamada, T.; Ponzovskaya Devine, E.; Elrefaie, A. F.; Wang, S.-Y.; Islam, M. S. Photon-trapping microstructures enable high-speed high-efficiency silicon photodiodes. *Nat. Photonics* **2017**, *11*, 301–308.
- (11) Kim, M.; Lee, G. J.; Choi, C.; Kim, M. S.; Lee, M.; Liu, S.; Cho, K. W.; Kim, H. M.; Cho, H.; Choi, M. K.; Lu, N.; Song, Y. M.; Kim, D.-H. An aquatic-vision-inspired camera based on a monocentric lens and a silicon nanorod photodiode array. *Nat. Electron.* **2020**, *3*, 546–553.
- (12) Kishino, K.; Unlu, M. S.; Chyi, J.-I.; Reed, J.; Arsenault, L.; Morkoc, H. Resonant cavity-enhanced (RCE) photodetectors. *IEEE J. Quantum Electron.* **1991**, *27*, 2025–2034.
- (13) Lechago, S.; García-Meca, C.; Griol, A.; Kovylyna, M.; Bellieres, L.; Martí, J. All-silicon on-chip optical nanoantennas as efficient interfaces for plasmonic devices. *ACS Photonics* **2019**, *6*, 1094–1099.
- (14) Kelzenberg, M. D.; Boettcher, S. W.; Petykiewicz, J. A.; Turner-Evans, D. B.; Putnam, M. C.; Warren, E. L.; Spurgeon, J. M.; Briggs, R. M.; Lewis, N. S.; Atwater, H. A. Enhanced absorption and carrier collection in Si wire arrays for photovoltaic applications. *Nat. Mater.* **2010**, *9*, 239–244.
- (15) Koepfli, S. M.; Baumann, M.; Koyaz, Y.; Gadola, R.; Güngör, A.; Keller, K.; Horst, Y.; Nashashibi, S.; Schwanninger, R.; Doderer, M.; Passerini, E.; Fedoryshyn, Y.; Leuthold, J. Metamaterial graphene photodetector with bandwidth exceeding 500 gigahertz. *Science* **2023**, *380*, 1169–1174.
- (16) Chen, D.; March, S. D.; Jones, A. H.; Shen, Y.; Dadey, A. A.; Sun, K.; McArthur, J. A.; Skipper, A. M.; Xue, X.; Guo, B.; Bai, J.; Band, S. R.; Campbell, J. C. Photon-trapping-enhanced avalanche photodiodes for mid-infrared applications. *Nat. Photonics* **2023**, *17*, 594–600.
- (17) Miao, X.; Yan, L.; Wu, Y.; Liu, P. Q. High-sensitivity nanophotonic sensors with passive trapping of analyte molecules in hot spots. *Light Sci. Appl.* **2021**, *10*, 5.
- (18) Wei, J.; Chen, Y.; Li, Y.; Li, W.; Xie, J.; Lee, C.; Novoselov, K. S.; Qui, C.-W. Geometric filterless photodetectors for mid-infrared spin light. *Nat. Photonics* **2023**, *17*, 171–178.
- (19) Hu, J.; Zhang, X.; Hu, C.; Sun, J.; Wang, X.; Lin, H.-Q.; Li, G. Correlated flat bands and quantum spin liquid state in a cluster Mott insulator. *Commun. Phys.* **2023**, *6*, 172.
- (20) Tang, E.; Mei, J.-W.; Wen, X.-G. High-temperature fractional quantum hall states. *Phys. Rev. Lett.* **2011**, *106*, 236802.
- (21) Suárez Morell, E.; Correa, J. D.; Vargas, P.; Pacheco, M.; Barticevic, Z. Flat bands in slightly twisted bilayer graphene: Tight-binding calculations. *Phys. Rev. B* **2010**, *82*, 121407.
- (22) Yang, Y.; Roques-Carnes, C.; Kooi, S. E.; Tang, H.; Beroz, J.; Mazur, E.; Kammer, I.; Joannopoulos, J. D.; Soljačić, M. Photonic flatband resonances for free-electron radiation. *Nature* **2023**, *613*, 42–47.
- (23) Vicencio, R. A.; Cantillano, C.; Morales-Inostroza, L.; Real, B.; Mejía-Cortés, C.; Weimann, S.; Szameit, A.; Molina, M. I. Observation of localized states in Lieb photonic lattices. *Phys. Rev. Lett.* **2015**, *114*, 245503.
- (24) Jacqmin, T.; Carusotto, L.; Sagnes, I.; Abbarchi, M.; Solnyshkov, D. D.; Malpuech, G.; Galopin, E.; Lemaître, A.; Bloch, J.; Amo, A. Direct observation of Dirac cones and a flatband in a honeycomb lattice for polaritons. *Phys. Rev. Lett.* **2014**, *112*, 116402.
- (25) Tang, H.; Ni, X.; Du, F.; Srikrishna, V.; Mazur, E. On-Chip Light trapping in bilayer Moiré photonic crystal slabs. *Appl. Phys. Lett.* **2022**, *121*, 231702.
- (26) Liang, Y.; Lin, H.; Lin, S.; Wu, J.; Li, W.; Meng, F.; Yang, Y.; Huang, X.; Jia, B.; Kivshar, Y. Hybrid anisotropic plasmonic metasurfaces with multiple resonances of focused light beams. *Nano Lett.* **2021**, *21*, 8917–8923.
- (27) Xiang, Y.; Zhai, Y.; Yuan, J.; Ren, K.; Zhao, X.; Wu, D.; La, J.; Wang, Y.; Wang, W. Amplified spontaneous emission at the band edges of Ag-coated Al nanocone array. *Photonics Res.* **2023**, *11*, 2202–2209.
- (28) Nguyen, H. S.; Dubois, F.; Deschamps, T.; Cuffe, S.; Pardon, A.; Leclercq, J.-L.; Seassal, C.; Letartre, X.; Viktorovitch, P. Symmetry breaking in photonic crystals: on-demand dispersion from flatband to Dirac cones. *Phys. Rev. Lett.* **2018**, *120*, 066102.
- (29) Wu, F.; Liu, T.; Long, Y.; Xiao, S.; Chen, G. Giant photonic spin Hall effect empowered by polarization-dependent quasibound states in the continuum in compound grating waveguide structures. *Phys. Rev. B* **2023**, *107*, 165428.
- (30) Cotrufo, M.; Cordaro, A.; Sounas, D. L.; Polman, A.; Alù, A. Passive bias-free non-reciprocal metasurfaces based on thermally nonlinear quasi-bound states in the continuum. *Nat. Photonics* **2024**, *18*, 81.
- (31) Munley, C.; Manna, A.; Sharp, D.; Choi, M.; Nguyen, H. A.; Cossairt, B. M.; Li, M.; Barnard, A. W.; Majumdar, A. Visible wavelength flatband in a gallium phosphide metasurface. *ACS Photonics* **2023**, *10*, 2456–2460.
- (32) Li, Q.; Van De Groep, J.; Wang, Y.; Kik, P. G.; Brongersma, M. L. Transparent multispectral photodetectors mimicking the human visual system. *Nat. Commun.* **2019**, *10*, 4982.
- (33) Li, R.; Whitmire, E.; Stengel, M.; Boudaoud, B.; Kautz, J.; Luebke, D.; Patel, S.; Aksit, K. Optical Gaze Tracking with Spatially-Sparse Single-Pixel Detectors; 2020 IEEE International Symposium on Mixed and Augmented Reality (ISMAR) 2020; pp 117–126.
- (34) Okamoto, T.; Kawata, S.; Minami, S. Fourier transform spectrometer with a self-scanning photodiode array. *Appl. Opt.* **1984**, *23*, 269.
- (35) Hijazi, M.; Huang, S.; Safari, M. Highly Sensitive SPAD-Based Receiver for Dimming Control in LiFi Networks. *Sensors* **2023**, *23*, 4673.
- (36) Selection guide/Si photodiodes, Hamamatsu Tech. Rep. Cat. No. KSPD0001E19 (2023).
- (37) Afzalian, A.; Flandre, D. Characterization of quantum efficiency, effective lifetime and mobility in thin film ungated SOI lateral PIN photodiodes. *Solid-State Electron.* **2007**, *51*, 337–342.
- (38) Afzalian, A.; Flandre, D. Physical Modeling and Design of Thin-Film SOI Lateral PIN Photodiodes. *IEEE Trans. Electron Devices* **2005**, *52*, 1116–1122.
- (39) Li, X.; Carey, J. E.; Sickler, J. W.; Pralle, M. U.; Palsule, C.; Vineis, C. J. Silicon photodiodes with high photoconductive gain at room temperature. *Opt. Express* **2012**, *20*, 5518.
- (40) Michel, A.-K. U.; Chigrin, D. N.; Maß, T. W. W.; Schönauer, K.; Salanga, M.; Wuttig, M.; Taubner, T. Using Low-Loss Phase-Change Materials for Mid-Infrared Antenna Resonance Tuning. *Nano Lett.* **2013**, *13*, 3470–3475.
- (41) Heßler, A.; Wahl, S.; Leuteritz, T.; Antonopoulos, A.; Stergianou, C.; Schön, C.-F.; Naumann, L.; Eicker, N.; Lewin, M.; Maß, T. W. W.; Wuttig, M.; Linder, S.; Taubner, T. In3SbTe2 as a programmable nanophotonics material platform for the infrared. *Nat. Commun.* **2021**, *12*, 924.
- (42) Slobodkin, Y.; Weinberg, G.; Hörner, H.; Pichler, K.; Rotter, S.; Katz, O. Massively degenerate coherent perfect absorber for arbitrary wavefronts. *Science* **2022**, *377*, 995–998.